Population Encoding by Circadian Clock Neurons Organizes Circadian Behavior

Christopher M Ciarleglio[1,2], **Karen L Gamble**[2], **John C Axley**[2], **Benjamin R Strauss**[2], **Jeremiah Y Cohen**[1], **Christopher S Colwell**[3], and **Douglas G McMahon**[1,2]

1 *Neuroscience Graduate Program, Vanderbilt University, Nashville, TN*

2 *Department of Biological Sciences, Vanderbilt University, Nashville, TN*

3 *Department of Psychiatry and Biobehavioral Sciences, UCLA, Los Angeles, CA*

Abstract

Mammalian circadian rhythms are orchestrated by the suprachiasmatic nuclei (SCN) of the hypothalamus. The SCN are composed of circadian clock neurons but the mechanisms by which these populations of neuronal oscillators encode rhythmic behavior are incompletely understood. We have used *ex vivo* real-time gene expression imaging of the neural correlates of circadian behavior, combined with genetic disruption of vasoactive intestinal polypeptide (VIP), a key SCN signaling molecule, to examine the neural basis of circadian organization in the SCN. We show that the coherence and timing of clock neuron rhythms are correlated with the coherence and timing of behavioral rhythms within individual mice, and that the degree of disruption of SCN neuronal organization correlates with the degree of behavioral disruption within individuals. Our results suggest that the SCN encode circadian phase as a temporal population vector of its constituent neurons such that as the neuronal population becomes desynchronized, phase information becomes ambiguous.

Keywords

VIP; Per1; suprachiasmatic nucleus; light; circadian; imaging

Introduction

The master circadian clock in mammals is a gene-driven neural network that temporally regulates behavior and physiology. It is composed of ca. 20,000 neurons, and is located in the suprachiasmatic nuclei of the hypothalamus (SCN) (Weaver, 1998). At a gross level, the SCN's control of circadian behavior is clearly established as SCN lesions result in behavioral circadian arrhythmicity (Stephan and Zucker, 1972; Moore and Eichler, 1976; Rusak, 1977) that can be restored by SCN transplants (Lehman et al., 1987). At a more refined level, it is unclear how neurons within the SCN neural network act to control or regulate circadian behavior.

Vasoactive intestinal polypeptide (VIP) is a key signaling molecule expressed in neurons of the retino-recipient region of the SCN, where it is rhythmically released in a light-cycle and can reset the phase of the clock in response to nighttime light pulses (Takahashi et al., 1989; Albers et al., 1990; Shinohara et al., 1993; Yang et al., 1993; Piggins et al., 1995; Ban et al.,

Corresponding Author: Douglas G. McMahon, Department of Biological Sciences, Vanderbilt University, 8270A MRBIII, 465 21st Ave. South, Nashville, TN 37232, w. (615) 936-3933, f. (615) 936-3932, E-mail: douglas.g.mcmahon@vanderbilt.edu.

1997). Mice lacking VIP-ergic signaling show marked circadian abnormalities such as an inability to phase shift in response to light pulses and blunted endogenous behavioral circadian rhythms (Harmar et al., 2002; Colwell et al., 2003). In addition, neonatal SCN from *VIP*^{-/-} mice exhibit reduced synchrony of neuronal spike frequency rhythms (Aton et al., 2005) and of neuronal clock gene expression of rhythms (Maywood et al., 2006). Manipulation of this SCN signaling molecule offers the opportunity to perturb SCN organization and to test the relationship between clock network organization and the control of behavior.

Using *ex vivo* real-time clock gene expression imaging of SCN networks and neurons in which SCN are acutely explanted and characterized from behaviorally characterized VIP-deficient mice, we sought to ascertain the aspects of SCN network organization that define behavioral circadian organization. Our findings indicate that within individual mice the degree of behavioral circadian disruption resulting from loss of VIP is correlated with the degree of desynchrony in the SCN neural network and that the onset of behavioral activity coincides with a specific phase of SCN rhythms. These results suggest that in the circadian clock, the overall pattern and organization of rhythmic neuronal activity that drives the temporal organization of locomotor behavior is encoded by the mean temporal population vector of SCN neuron rhythms.

Methods

Animals and housing

Mice with a targeted *VIP* gene disruption (Colwell et al., 2003) were backcrossed four generations to mice (B6C3 hybrid from Jackson Labs) carrying the *mPer1*::d2EGFP transgene (Kuhlman et al., 2000) yielding *Per1*::GFP^{+/+}, *VIP*^{+/-} mice which were bred in a 12L:12D light-cycle (LD) to yield experimental mice. Male offspring 3-5 weeks of age were placed in litter-filled wheel cages (Coulbourn Instruments, Whitehall, PA) with food and water *ad libitum*. All mice were entrained to 12L:12D light-cycles for 9-22 days, and then either euthanized and their SCN explanted to assay SCN molecular rhythms *ex vivo* as part of the LD experimental group, or maintained in constant darkness (DD) for an additional 20-60 days and then euthanized and their SCN explanted to assay SCN rhythms *ex vivo* as part of the DD group. Animals were euthanized by cervical dislocation between Zeitgeber Time (ZT) 9-12 in LD (where ZT 12 is lights-off), or Circadian Time (CT) 9-13 in DD (where CT 12 is the onset of activity). Behavioral onset of mice behaviorally arrhythmic in DD could not be assigned. They were euthanized along with their rhythmic counterparts and their SCN rhythm phases are reported as time *ex vivo*. All animal care was conducted in accordance with Vanderbilt University IACUC guidelines.

Behavioral analyses

Wheel-running activity was monitored and recorded in 5-minute bins using ClockLab software (Actimetrics, Evanston, IL). Behavior was analyzed using ClockLab Analysis software, and activity was quantified as the number of wheel revolutions occurring during 5-min bins. In LD, the proportions of activity during lights-on and lights-off, as well as the total amount of activity per day were determined for the last 9 days in LD using the "activity profile" function. In DD, activity was measured for the first 20 days in darkness. Chi-squared periodogram analysis yielded rhythmic power as a measure of the amplitude and coherence of behavioral rhythms (Colwell et al., 2003). Linear regression (Pittendrigh and Daan, 1976) was also used to project behavioral onset (CT12) in rhythmic animals to establish a consistent time of euthanization (CT 9-13).

Ex vivo culture

After behavioral characterization, mouse brains were extracted and blocked in cold sampling media as previously described (Ohta et al., 2006). One or two 200-μm coronal hypothalamic sections per animal were made on a Vibroslicer (Campden Instruments, Lafayette, IN). SCN were isolated by trimming the surrounding hypothalamic tissue and placed on a Millicell (Millipore) culture membrane insert in 37°C recording media (Ohta et al., 2006), conditioned with GIBCO N-2 supplement (Invitrogen, Carlsbad, CA) and contained in 35-mm culture dishes (Falcon, BD, Franklin Lakes, NJ). Dishes were then sealed with sterile high-vacuum grease and placed in a custom 6-well aluminum chamber heated to 35.5°C by a voltage-regulator.

Confocal imaging

The 6-well chamber containing cultured slices was placed on an automated stage on a laser-scanning confocal microscope (LSM5 PASCAL, Zeiss, Germany) with GFP excitation at 488 nm, and bandpass emission recorded between 505-555 nm. Three Z-stack images totaling 40-μm in depth were taken of each slice every hour for 90 hours. Focus was adjusted manually to account for slice swelling and flattening as needed.

Ex vivo analyses

Raw LSM files of SCN time-lapse imaging were compiled in MetaMorph (Molecular Devices, Downingtown, PA). The Z-stack for each time-point was compressed into a single maximum projection image from which a background subtraction was made (Close-Open morphological filter with a 75 pixel-round sequential average). Whole SCN or single cells were selected as regions of interest (ROI) from the resultant time-series stack, and time-lapse intensity measurements were made and exported to an in-house program created in R (http://www.r-project.org/) that allowed selection of minima and maxima for each SCN or cell, and calculation of phase. The first 12 hours *ex vivo* were omitted from the analyses. Peaks in fluorescence were visually scored as having a clear rising and falling phase above baseline fluorescence, and the number of circadian peaks per SCN or per cell was determined by 3-person independent visual scoring. For the purposes of this study, SCN or cells with two or more peaks were considered rhythmic. Overall slice fluorescence was determined by the total integrated fluorescence over hours 12-36 *ex vivo* divided by the area.

Statistical analysis

Circular statistics and Rayleigh vector plots were performed in Oriana 2.0 (Rockware, Golden, CA). Statistics were calculated for each animal for further comparison. Means were statistically compared in SPSS 14.0 (SPSS, Chicago, IL) with independent samples *t*-tests (two-tailed) and one-way analyses of variance (ANOVA) followed by post-hoc Fisher's Least Significant Difference tests, except for when the variances were not homogeneous, as indicated by a significant Levene's test. In these cases, nonparametric Kruskal-Wallis or Median tests were used. For correlational analysis, Pearson's product moment correlations were used. Significance was ascribed at $p < 0.05$.

Results

VIP^{-/-} Per1::GFP mice exhibit weakened, phase advanced circadian behaviors

VIP knockout mice have been previously shown to exhibit specific circadian behavioral deficits, including altered light entrainment in LD and disrupted free-running circadian rhythms in DD (Colwell et al., 2003). To confirm that these traits persisted following breeding onto the *Per1*::GFP circadian reporter background, we examined the circadian behavior of VIP knockout (VIP$^{-/-}$), heterozygous (VIP$^{+/-}$) and wildtype (VIP$^{+/+}$) *Per1*::GFP mice in LD and

DD (Fig. 1). In light/dark cycles all genotypes exhibited primarily nocturnal locomotor patterns, but VIP$^{-/-}$ mice had less robust partitioning of activity into the night (dark) portion of the cycle, performing a greater percentage of wheel-running during the light-phase than the other genotypes (Median test, $\chi^2(2) = 3.76$, $p < 0.05$, Fig. 1A, C). In constant darkness VIP$^{-/-}$ mice exhibited severely disrupted free running circadian behavior compared to wildtype and heterozygous mice. They lacked clear, coherent circadian rhythms (Fig. 1B), and exhibited a significant reduction in rhythmic power in periodogram analysis ($F(2, 22) = 13.4$, $p < 0.01$, Fig. 1D). At the transition from LD into DD, many *VIP$^{-/-}$* mice did exhibit an initial behavioral onset during the first day in DD that was phase advanced by 5-6 hours compared to the onsets of *VIP$^{+/-}$* and *VIP$^{+/+}$* mice (Kruskal-Wallis, $\chi2(2) = 8.8$, $p < 0.05$, Fig. 1E). These results demonstrate that the signature circadian deficits associated with the lack of VIP signaling in the SCN—weakened light entrainment, disrupted endogenous rhythms and advanced phase angle of activity onset (Colwell et al., 2003)—are preserved in *VIP$^{-/-}$Per1*::GFP mice.

VIP$^{/-}$Per1::GFP mice exhibit desynchronized, phase advanced SCN neuronal rhythms

We next characterized the SCN organization of the mice behaviorally characterized in Fig. 1 by measuring circadian rhythms in the expression of *Per1* promoter-driven short half-life GFP in acute, *ex vivo* hypothalamic slice culture (Kuhlman et al., 2000;Quintero et al., 2003;Ohta et al., 2005;Ohta et al., 2006). After behavioral characterization in LD or DD, coronal SCN slices from each mouse were acutely explanted into organotypic slice culture. Cultures were imaged hourly for 90 hours on a confocal microscope, providing an assay of SCN network organization that could then be correlated with the animal's previous behavior, genotype and lighting condition.

Fig. 2A-C (and Supplementary Movies 1 and 2) show the SCN tissue and the SCN neuron *Per1*::GFP rhythms from the individual mice that were behaviorally characterized in Fig. 1. Each column shows imaging data from an individual mouse matching the corresponding genotype and condition in Fig. 1 (i.e., the data in the LD, *VIP$^{+/+}$* column in Fig. 2A-C are imaging data from the SCN explant of the mouse for which the behavioral record is Fig. 1A LD, *VIP$^{+/+}$*, etc.). Overall SCN rhythmicity, as measured by the integrated *Per1*::GFP fluorescence of the SCN, was robustly rhythmic in explants from *VIP$^{+/+}$* and *VIP$^{+/-}$* mice in LD and DD, but was significantly disrupted in *VIP$^{-/-}$* explants in both LD and DD (Fig. 2A). Like locomotor behavior of *VIP$^{-/-}$* mice at the LD to DD transition, *Per1*::GFP gene expression in explants from LD *VIP$^{-/-}$* mice often exhibited a detectable initial onset cycle, followed by damped or disrupted rhythmicity during subsequent cycles *ex vivo* (Fig. 2A), suggesting that de-afferentation of the explant may mimic the LD to DD transition. SCN explants from *VIP$^{-/-}$* mice maintained in DD exhibited disrupted tissue-level circadian rhythms (Fig. 2A) similar to their disrupted circadian behavior (Fig. 1A).

At the cellular level, individual SCN neurons exhibited robust circadian rhythms in reporter gene expression in explants from all genotypes maintained in both LD and DD, even in *VIP$^{-/-}$* mice with disrupted behavioral and SCN rhythms. Figure 2B shows all the cellular rhythms from the corresponding SCN slices in Fig. 2A, whereas Supplementary Fig. 1 shows a limited number of typical cellular rhythms from the same slices to better illustrate the properties of individual cellular rhythms. Rayleigh vector plots of the distribution of neuronal *Per1*::GFP rhythm phases revealed that the degree of synchrony in neuronal rhythms—as shown by vector arrow length—was reduced in *VIP$^{-/-}$* mouse explants, particularly in DD (Fig. 2C). Further quantitative analysis of the imaging data showed that in explants from mice maintained in LD, there was a trend toward increased neuronal phase variance within each mouse as the number of functional *VIP* alleles decreased, with *VIP$^{-/-}$* explants exhibiting the highest degree of neuronal phase variance ($F(2, 10) = 2.0$, $p = 0.19$, Fig. 2D). Similarly, in explants from mice in DD, the variance of the individual cell phases within each animal was

significantly greater in $VIP^{-/-}$ explants than in $VIP^{+/+}$ explants (Kruskal-Wallis, $\chi 2(2) = 9.171$, $p = 0.01$, Fig. 2E). Finally, the onset phase (10% rise) of the first $Per1$::GFP cycle $ex\ vivo$ occurred 5-6 hours earlier in $VIP^{-/-}$ SCN compared to $VIP^{+/-}$ and $VIP^{+/+}$ SCN ($F(2,21) = 4.1$, $p<0.05$, Fig. 2F), similar to the onset of behavioral rhythms at the LD to DD transition. The lack of detectable synchrony in SCN neuronal phases across slices from $VIP^{-/-}$ mice in DD (Supplementary Fig. 2), in which the time axis is hours $ex\ vivo$, indicated that dissection and transition to $ex\ vivo$ conditions did not set neuronal phase.

SCN neuronal phase distribution sets behavioral coherence and timing

Given the striking correspondence of changes in the neuronal phase distribution with alterations in circadian behavior that we observed across mouse populations with altered VIP communication, we next tested if SCN neuronal phase organization was correlated with circadian behavioral characteristics within individual mice across VIP genotype and lighting condition. Indeed, the proportion of wheel-running activity that occurred during the light-phase of LD cycles was significantly and positively correlated with increased neuronal phase variance within individual animals across all genotypes (i.e., increased daytime activity was associated with decreased neuronal synchrony in all mice; $r (15) = 0.568$, $p < 0.05$, Fig. 3A). Similarly, behavioral rhythmic power was significantly and negatively correlated with neuronal phase variance within individual animals across VIP gene dosage (i.e., decreased behavioral rhythmic power was associated with increased neuronal desynchrony in all mice; $r (18) = -0.641$, $p < 0.01$, Fig. 3B). In addition to the correlations of neuronal phase variance with the coherence of behavioral rhythms, the timing of molecular rhythms in the SCN neural network also correlated with the timing of behavioral activity. In SCN from mice maintained in LD, both the onset of the $Per1$::GFP rhythm (10% above baseline on the rising phase) during the first cycle $ex\ vivo$ and the onset of behavioral activity during the first cycle in DD were phase advanced by 5-6 hours in $VIP^{-/-}$ mice compared to other genotypes (Fig.3C).

Whereas the characteristics of circadian behavior mirrored SCN neuronal phase distribution and onset time, there was no significant correlation between other aspects of SCN rhythms and circadian behavior. Overall levels of $Per1$::GFP expression, measured as fluorescence intensity, were similar across VIP genotypes ($F(2, 70) = 1.359$, $p = 0.26$) and there was no correlation between the number or percent of rhythmic neurons in an individual animal's SCN explant and the behavioral rhythmic power of that mouse in DD (Pearson's product moment correlation for: number, $r (20) = 0.255$, $p = 0.28$ and percent, $r (20) = 0.238$, $p = 0.31$). Furthermore, the percentage of rhythmic neurons in individual SCN explants was similar across VIP genotypes and across lighting conditions (LD: $F(2, 11) = 2.7$, $p = 0.11$; DD: $F(2, 18) = 1.3$, $p = 0.29$, Fig. 3D and Supplementary Fig. 3).

Discussion

In this study, we have disrupted SCN network organization by targeted deletion of a key communicating molecule, VIP, and then assayed the circadian behavior and the neural correlates of circadian behavior by $ex\ vivo$ real-time gene expression imaging of circadian clock neurons in the SCN of individual mice. Our principal findings are that the timing (phase) and coherence (power) of circadian behavior is encoded by the timing and degree of synchrony of SCN neuronal rhythms. The timing and strength of circadian locomotor rhythms is encoded by the timing and strength of the SCN average neuronal temporal population vector.

Targeted knockout of the VIP gene disrupts the circadian neural network by leading to neuronal de-synchronization and results in stereotypical behavioral deficits such as increased daytime wheel running and arrhythmicity in constant darkness. In this study, we found that the weakened behavioral rhythms and phase-advanced DD behavioral onset in adult $VIP^{-/-}Per1$::GFP mice reflect the less synchronized and phase advanced patterns of neural

rhythms recorded *ex vivo* in the SCN of the same individual animals. Specifically, the degree of degradation of behavioral rhythmic coherence was correlated with the degree of degradation of rhythmic coherence in the population of SCN neurons within an individual (Fig. 3A, B). We also found that the first peak of SCN network *Per1*::GFP expression maintains a constant phase relationship to activity onset across *VIP* genotypes, with the initial rise in gene activity anticipating behavioral activity onset by 7-8 hours and matching the 5-6 hour phase advance of activity in the $VIP^{-/-}$ mice. Unexpectedly, we also found that while SCN neuronal synchrony was disrupted in $VIP^{-/-}$ mice, SCN neurons from $VIP^{-/-}$ mice exhibited robust rhythmicity in similar number and proportion to SCN neuronal molecular rhythms from $VIP^{+/-}$ and $VIP^{+/+}$ mice.

There are both similarities and differences between our results and the results from previous circadian studies using VIP communication-deficient mice. Our study used acutely explanted, *ex vivo* SCN from adult $VIP^{-/-}$ mice to assay circadian behavior and establish circadian neural correlates within individual mice. In contrast, previous studies used reconstituted dispersed neonatal SCN networks or reorganized neonatal SCN explants that had been maintained chronically *in vitro* for 2 or more weeks before recording, and then inferred a relationship of *in vitro* findings to adult circadian behavior based on genotype (Aton et al., 2005; Maywood et al., 2006). Our finding that compromised VIP signaling leads to de-synchronization of SCN clock neurons is in accordance with studies of neonatal SCN networks, and strengthens the conclusion that VIP acts as a synchronizing substance in the SCN (Aton et al., 2005; Maywood et al., 2006; Brown et al., 2007). In addition, we have now demonstrated directly the previous speculation that the de-synchronization of SCN neurons is accompanied by loss of behavioral rhythmic coherence within individuals. Our results demonstrating preservation of the number and proportion of individual neuronal rhythms in explanted adult $VIP^{-/-}$ SCN stand in contrast to the neonatal VIP studies in which there was significant loss in the proportion of rhythmic neurons following loss of VIP communication in SCN networks (Aton et al., 2005; Maywood et al., 2006). A study of VIP receptor knockout adult animals also revealed a surprisingly high proportion of rhythmic but desynchronized SCN neurons (Hughes et al., 2008). The reasons for these differences are unknown, but could be explained by a number of factors including a difference in the role of VIP in mature vs. neonatal SCN networks, differences in culture time (4 days vs. 2-3 weeks), access to a running wheel or compensation in the adult by upregulation of other signaling molecules in the SCN network such as GRP that could sustain cellular rhythms (Maywood et al., 2006). Whatever the precise cause, it is clear that one inference drawn from the neonatal SCN studies, that cellular de-synchronization in the SCN necessarily leads to reduced cellular rhythmicity, does not hold in the case of VIP communication, or in the case of disruption of SCN neuronal synchrony by constant light, where cellular rhythm robustness is also preserved in the face of cellular desynchrony (Ohta et al., 2005; Ohta et al., 2006).

Our findings have significant implications for understanding how the SCN neural network encodes and drives circadian behavior. The present study of *VIP* gene-dosage effects, in combination with work on mice exposed to constant light (Ohta et al., 2005; Ohta et al., 2006), demonstrates a strong correlation between the timing and coherence of circadian locomotor behavior, and the timing and coherence of neuronal phases within the SCN, represented as the temporal direction and magnitude of the population vector of SCN neuronal rhythms. Work on neonatal SCN and SCN neurons from *Tau*-mutant hamsters and *Clock$^{\Delta 19}$*-mutant mice, has suggested that behavioral circadian period is approximated by the population average period of the individual neurons that comprise the SCN (Liu et al., 1997; Herzog et al., 1998). Similarly, chimeric SCN composed of wildtype and *Clock$^{\Delta 19}$*-mutant SCN neurons drive circadian behavior with the intrinsic period of the majority of neurons (Low-Zeddies and Takahashi, 2001). The present data suggest that, similar to period, the timing (phase) of behavioral onset is encoded by the average phase of the neural population represented as a

temporal population vector with the temporal direction of the vector determining the time of activity onset and the magnitude of the vector determining the coherence of the behavioral rhythms. In this way, the manner in which the circadian network encodes behavioral phase is not unlike the population coding observed in the voluntary motor system, in which the spatial direction of targeted limb movements is coded by the average population vector of directional motor neurons in the cortex (Georgopoulos et al., 1986).

This concept of population encoding can be extended to the paired SCN and to multiple neuronal populations within each SCN to account for exceptional circumstances in which SCN neuronal sub-populations can encode bimodal circadian behavioral output. For example, "splitting" of behavioral circadian rhythms in response to constant light correlates with antiphase oscillation of the gene expression rhythms in the SCN neurons of the paired SCN (de la Iglesia et al., 2000; Ohta et al., 2005). Similarly, seasonal light cycles induce changes in the distribution of neuronal phases within the SCN (Inagaki et al., 2007; VanderLeest et al., 2007; Naito et al., 2008) that likely encode for photoperiodic changes in circadian behaviors. Population coding in the SCN has these potential advantages: 1) the summation of neuronal phases may lead to greater accuracy and precision of circadian behavioral activity onset similar to the increase in precision of period gained by population encoding (Liu et al., 1997; Herzog et al., 1998); 2) a network composed of neurons with variable phase relationship and a population encoded output to behavior can flexibly encode the amplitude and phase of changing environmental stimuli (such as seasonal light cycles) and through the phase organization of the neuronal population, drive circadian behavior appropriately. VIP is a signal for light stimuli within the SCN network as well as a synchronizing agent (Piggins et al., 1995; Aton et al., 2005; Maywood et al., 2006). Thus, the overall role of VIP communication in the SCN appears to be to modulate the timing and coherence of population vector encoding by SCN neurons to adjust circadian behavior to environmental light input.

Supplementary Material

Refer to Web version on PubMed Central for supplementary material.

Acknowledgements

References

Albers HE, Stopa EG, Zoeller RT, Kauer JS, King JC, Fink JS, Mobtaker H, Wolfe H. Day-night variation in prepro vasoactive intestinal peptide/peptide histidine isoleucine mRNA within the rat suprachiasmatic nucleus. Brain Res Mol Brain Res 1990;7:85–89. [PubMed: 2153898]

Aton SJ, Colwell CS, Harmar AJ, Waschek J, Herzog ED. Vasoactive intestinal polypeptide mediates circadian rhythmicity and synchrony in mammalian clock neurons. Nat Neurosci 2005;8:476–483. [PubMed: 15750589]

Ban Y, Shigeyoshi Y, Okamura H. Development of vasoactive intestinal peptide mRNA rhythm in the rat suprachiasmatic nucleus. J Neurosci 1997;17:3920–3931. [PubMed: 9133410]

Brown TM, Colwell CS, Waschek JA, Piggins HD. Disrupted neuronal activity rhythms in the suprachiasmatic nuclei of vasoactive intestinal polypeptide-deficient mice. J Neurophysiol 2007;97:2553–2558. [PubMed: 17151217]

Colwell CS, Michel S, Itri J, Rodriguez W, Tam J, Lelievre V, Hu Z, Liu X, Waschek JA. Disrupted circadian rhythms in VIP- and PHI-deficient mice. Am J Physiol Regul Integr Comp Physiol 2003;285:R939–949. [PubMed: 12855416]

de la Iglesia HO, Meyer J, Carpino A Jr, Schwartz WJ. Antiphase oscillation of the left and right suprachiasmatic nuclei. Science 2000;290:799–801. [PubMed: 11052942]

Georgopoulos AP, Schwartz AB, Kettner RE. Neuronal population coding of movement direction. Science 1986;233:1416–1419. [PubMed: 3749885]

Harmar AJ, Marston HM, Shen S, Spratt C, West KM, Sheward WJ, Morrison CF, Dorin JR, Piggins HD, Reubi JC, Kelly JS, Maywood ES, Hastings MH. The VPAC(2) receptor is essential for circadian function in the mouse suprachiasmatic nuclei. Cell 2002;109:497–508. [PubMed: 12086606]

Herzog ED, Takahashi JS, Block GD. Clock controls circadian period in isolated suprachiasmatic nucleus neurons. Nat Neurosci 1998;1:708–713. [PubMed: 10196587]

Hughes AT, Guilding C, Lennox L, Samuels RE, McMahon DG, Piggins HD. Live Imaging of Altered Period1 Expression in the Suprachiasmatic Nuclei of Vipr2(-/-) Mice. J Neurochem. 2008

Inagaki N, Honma S, Ono D, Tanahashi Y, Honma K. Separate oscillating cell groups in mouse suprachiasmatic nucleus couple photoperiodically to the onset and end of daily activity. Proc Natl Acad Sci U S A 2007;104:7664–7669. [PubMed: 17463091]

Kuhlman SJ, Quintero JE, McMahon DG. GFP fluorescence reports Period 1 circadian gene regulation in the mammalian biological clock. Neuroreport 2000;11:1479–1482. [PubMed: 10841361]

Lehman MN, Silver R, Gladstone WR, Kahn RM, Gibson M, Bittman EL. Circadian rhythmicity restored by neural transplant. Immunocytochemical characterization of the graft and its integration with the host brain. J Neurosci 1987;7:1626–1638. [PubMed: 3598638]

Liu C, Weaver DR, Strogatz SH, Reppert SM. Cellular construction of a circadian clock: period determination in the suprachiasmatic nuclei. Cell 1997;91:855–860. [PubMed: 9413994]

Low-Zeddies SS, Takahashi JS. Chimera analysis of the Clock mutation in mice shows that complex cellular integration determines circadian behavior. Cell 2001;105:25–42. [PubMed: 11301000]

Maywood ES, Reddy AB, Wong GK, O'Neill JS, O'Brien JA, McMahon DG, Harmar AJ, Okamura H, Hastings MH. Synchronization and maintenance of timekeeping in suprachiasmatic circadian clock cells by neuropeptidergic signaling. Curr Biol 2006;16:599–605. [PubMed: 16546085]

Moore RY, Eichler VB. Central neural mechanisms in diurnal rhythm regulation and neuroendocrine responses to light. Psychoneuroendocrinology 1976;1:265–279. [PubMed: 792940]

Naito E, Watanabe T, Tei H, Yoshimura T, Ebihara S. Reorganization of the suprachiasmatic nucleus coding for day length. J Biol Rhythms 2008;23:140–149. [PubMed: 18375863]

Ohta H, Yamazaki S, McMahon DG. Constant light desynchronizes mammalian clock neurons. Nat Neurosci 2005;8:267–269. [PubMed: 15746913]

Ohta H, Mitchell AC, McMahon DG. Constant light disrupts the developing mouse biological clock. Pediatr Res 2006;60:304–308. [PubMed: 16857759]

Piggins HD, Antle MC, Rusak B. Neuropeptides phase shift the mammalian circadian pacemaker. J Neurosci 1995;15:5612–5622. [PubMed: 7643205]

Pittendrigh C, Daan S. A Functional Analysis of Circadian Pacemakers in Nocturnal Rodents: V. Pacemaker Structure: A Clock for All Seasons. J Comp Physiol 1976;106:333–355.

Quintero JE, Kuhlman SJ, McMahon DG. The biological clock nucleus: a multiphasic oscillator network regulated by light. J Neurosci 2003;23:8070–8076. [PubMed: 12954869]

Rusak B. Role of Suprachiasmatic Nuclei in Generation of Circadian-Rhythms in Golden-Hamster, Mesocricetus-Auratus. Journal of Comparative Physiology 1977;118:145–164.

Shinohara K, Tominaga K, Isobe Y, Inouye ST. Photic regulation of peptides located in the ventrolateral subdivision of the suprachiasmatic nucleus of the rat: daily variations of vasoactive intestinal polypeptide, gastrin-releasing peptide, and neuropeptide Y. J Neurosci 1993;13:793–800. [PubMed: 8426236]

Stephan FK, Zucker I. Circadian rhythms in drinking behavior and locomotor activity of rats are eliminated by hypothalamic lesions. Proc Natl Acad Sci U S A 1972;69:1583–1586. [PubMed: 4556464]

Takahashi Y, Okamura H, Yanaihara N, Hamada S, Fujita S, Ibata Y. Vasoactive intestinal peptide immunoreactive neurons in the rat suprachiasmatic nucleus demonstrate diurnal variation. Brain Res 1989;497:374–377. [PubMed: 2684344]

VanderLeest HT, Houben T, Michel S, Deboer T, Albus H, Vansteensel MJ, Block GD, Meijer JH. Seasonal encoding by the circadian pacemaker of the SCN. Curr Biol 2007;17:468–473. [PubMed: 17320387]

Weaver DR. The suprachiasmatic nucleus: a 25-year retrospective. J Biol Rhythms 1998;13:100–112. [PubMed: 9554572]

Yang J, Cagampang FR, Nakayama Y, Inouye SI. Vasoactive intestinal polypeptide precursor mRNA exhibits diurnal variation in the rat suprachiasmatic nuclei. Brain Res Mol Brain Res 1993;20:259–262. [PubMed: 8302164]
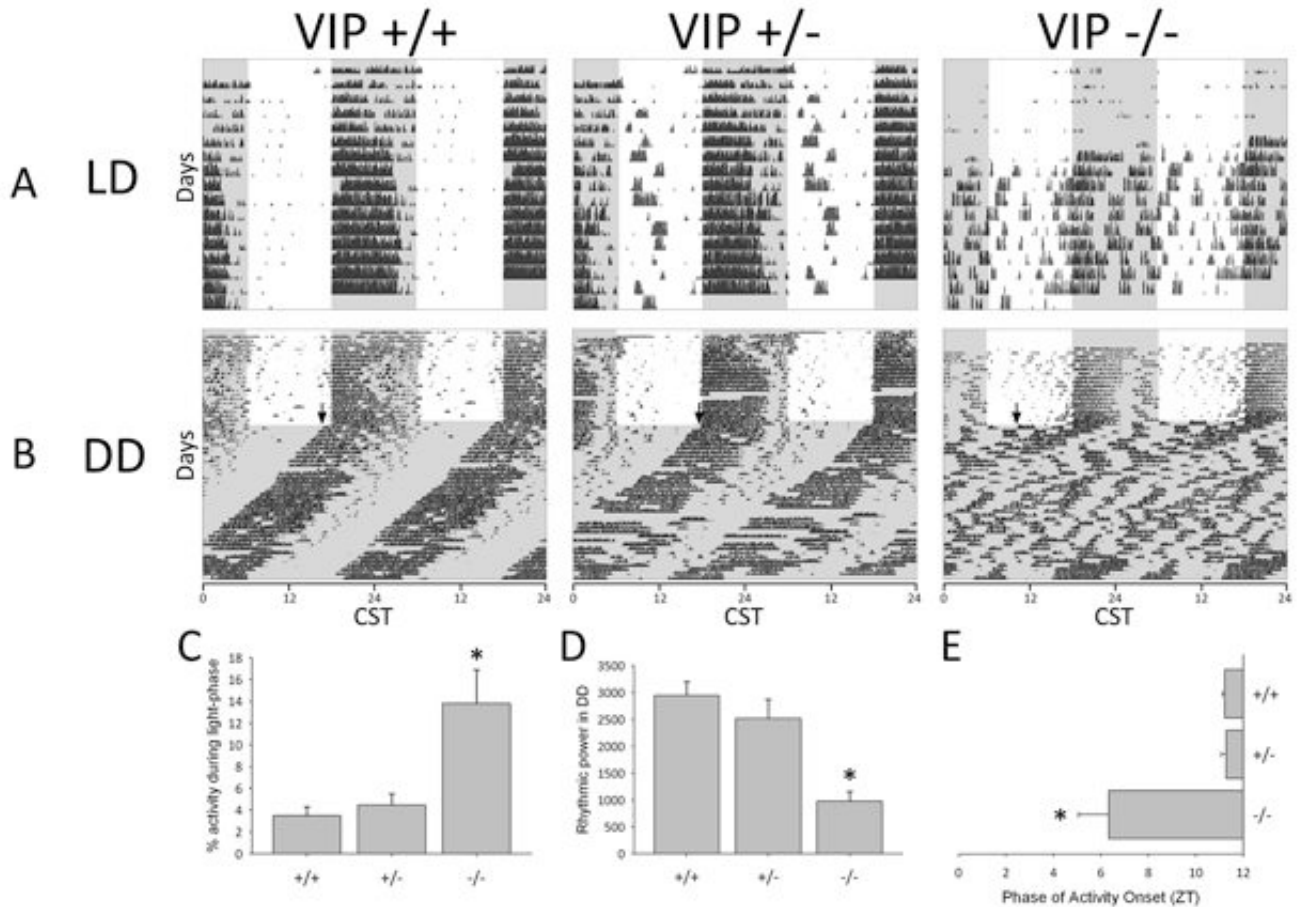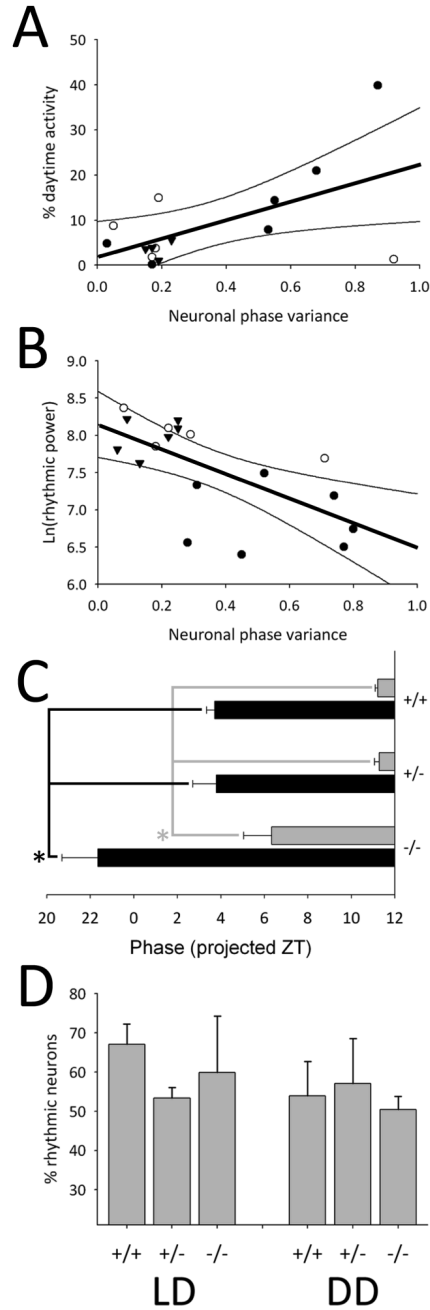
Figure 1.
VIP knockout *Per1*∷GFP mice exhibit altered circadian behavior. Left to right: example *VIP* wildtype (+/+), heterozygous (+/-) and knockout mice (-/-) on the *Per1*∷GFP reporter background. (*A*) Double-plotted actograms illustrate circadian behavior in a 12L:12D light cycle (LD). CST indicates Central Standard Time. (*B*) Double-plotted actograms illustrate circadian behavior in constant darkness (DD). Black arrow represents the phase of activity onset on the first day in DD. (*A, B*) Black ticks represent activity in 5-minute bins; white background denotes lights-on; gray background denotes lights-off. (*C*) Percentage of total wheel-running activity during the light-phase in LD for $VIP^{+/+}$ (N = 14), $VIP^{+/-}$ (N = 16) and $VIP^{-/-}$ (N = 16) mice. (*D*) Rhythmic power in constant darkness as measured by χ^2 periodogram amplitude for $VIP^{+/+}$ (N = 8), $VIP^{+/-}$ (N = 9) and $VIP^{-/-}$ (N = 8) mice. (*E*) Time of activity onset on the first day in constant darkness for $VIP^{+/+}$ (N = 7), $VIP^{+/-}$ (N = 9) and $VIP^{-/-}$ (N = 8) mice. Error bars represent SEM; asterisks (*) represent significance at *p* < 0.05.
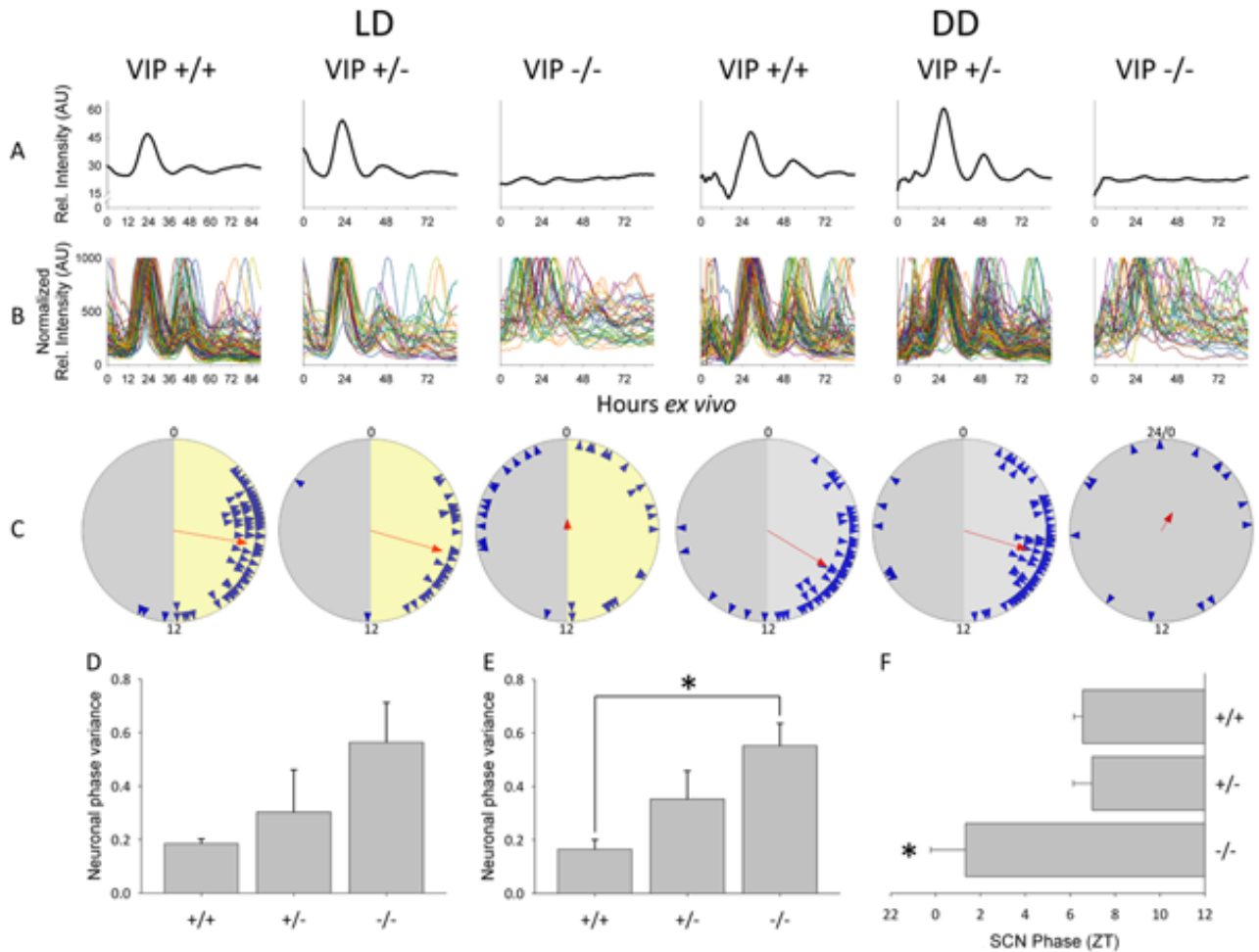
Figure 2.
Ex vivo circadian gene expression rhythms from SCN and clock neurons. Left to right: example *ex vivo* SCN *Per1*::GFP imaging data from *VIP* wildtype (+/+), heterozygous (+/-) and knockout mice (-/-). (**A**) Representative relative fluorescence intensity plots of *ex vivo* SCN for each of the *VIP* genotypes from LD (*left*) and DD (*right*) over 90 hours. (**B**) Representative normalized relative fluorescence intensity plots of individual neurons over 90 hours *ex vivo*. (**C**) Rayleigh plots from LD (*left*) and DD (*right*). Blue arrowheads represent the 50% peak rising phases of individual rhythmic neurons from a representative mouse of a particular genotype. Red arrow indicates the mean phase vector of rhythmic neurons, where length is inversely proportional to the neuronal phase variance, and the direction indicates timing relative to the previous light cycle in LD or previous behavioral cycles in DD. For LD (*left*), numbers indicate projected ZT, where projected ZT 0-12 is represented with a yellow background and projected ZT 12-24(0) is represented with a gray background; for DD (*right*), numbers indicate CT, where CT 0-12 is represented with a light gray background and CT 12-24(0) is represented with a darker gray background. For the *VIP*⁻/⁻ mouse in DD, in which CT could not be reliably assigned, the phases of neurons are plotted as time *ex vivo*. (**D**) Neuronal phase variance in SCN from *VIP*⁺/⁺ (N = 4), *VIP*⁺/⁻ (N = 5) and *VIP*⁻/⁻ (N = 4) mice maintained in LD. (**E**) Neuronal phase variance in SCN from *VIP*⁺/⁺ (N = 7), *VIP*⁺/⁻ (N = 8) and *VIP*⁻/⁻ (N = 7) mice maintained in DD. (**F**) SCN phase from *VIP*⁺/⁺ (N = 9), *VIP*⁺/⁻

(N = 9) and *VIP*^{-/-} (N = 6) mice previously maintained in LD. Error bars represent SEM; asterisks (*) represent significance at $p < 0.05$.

Figure 3.
Correlation of SCN neuronal rhythms with behavioral characteristics. (*A*) Plot of % daytime wheel-running activity vs. neuronal phase variance for individual mice (N = 15) by *VIP* genotype maintained in LD. (*B*) Plot of rhythmic power vs. neuronal phase variance for individual mice (N = 18) by *VIP* genotype maintained in DD. (*A, B*) Closed circles represent *VIP*$^{-/-}$ mice, open circles represent *VIP*$^{+/-}$ mice and triangles represent *VIP*$^{+/+}$ mice. Thick black line represents single order regression, and the thin black lines represent the 95% confidence interval. (*C*) Phase of SCN *Per1*::GFP onset (10% rising phase) on the first day *ex vivo* from mice maintained in LD (black bars) and onset of behavioral activity on the first day in DD (gray bars). For number of animals, see Fig. 1E and Fig. 2F. (*D*) Plot of the percent of rhythmic

neurons (2+ peaks) per SCN slice for mice maintained in LD (*left*) or in DD (*right*). LD: *VIP*$^{+/+}$ (N = 5), *VIP*$^{+/-}$ (N = 5) and *VIP*$^{-/-}$ (N = 4); DD: *VIP*$^{+/+}$ (N = 6), *VIP*$^{+/-}$ (N = 8) and *VIP*$^{-/-}$ (N = 7). Error bars represent SEM; asterisks (*) represent significance at $p < 0.05$.